Spin dynamics of high-spin fermions in optical superlattices

Shaobing Zhu (朱少兵)[1,2], Jun Qian (钱 军)[1], and Yuzhu Wang (王育竹)[1,*]

[1]*Key Laboratory for Quantum Optics and Center for Cold Atom Physics, Shanghai Institute of Optics and Fine Mechanics, Chinese Academy of Sciences, Shanghai 201800, China*

[2]*University of Chinese Academy of Sciences, Beijing 100049, China*

**Corresponding author: yzwang@mail.shcnc.ac.cn*

Received December 6, 2016; accepted March 3, 2017; posted online March 22, 2017

We investigate the spin dynamics, starting from the initial band-insulating state, of fermionic high-spin atoms in optical superlattices. Through numerical simulations and analytical calculations, we determine the time evolution behavior of the system. When the spin-changing strength and tunneling strength are comparable, the spin dynamics feature a spin-changing oscillation with the amplitude modulated by the superexchange interaction. When the double-well potential is very shallow, the spin dynamics feature a simple harmonic oscillation with the oscillation frequencies related only to the spin-changing strength, which can be properly explained with the perturbation model.

OCIS codes: 020.3320, 020.7010, 020.2070.

doi: 10.3788/COL201715.060202.

Fermionic atoms with high spin ($s > 1/2$) in optical lattices[1–4] provide a powerful and controllable platform for developing physical systems that go beyond the traditional spin 1/2 magnetism and for enabling an understanding of fundamental spin–spin interactions[5–9]. Widespread attention has been paid to the exploration of spin-changing collisions[10–14], the realization of exotic quantum phases[15–21], and the simulation of SU(N) magnetism[22–27]. The recent experimental realization of a well-controlled fermionic spinor gas of ^{40}K atoms with long-lived coherent spin dynamics has opened up a new route to investigate high-spin magnetism and multiflavor spin systems[8]. In addition, as the underlying mechanism of quantum magnetism, superexchange (or its low-order version, tunneling) has attracted extensive interest in the context of ultracold quantum gas in optical lattices[28–32]. For the fermionic high-spin system, the complex interplay of spin and the spatial degrees of freedom leads to instability of the initial band-insulating state and complicated many-body dynamics[8]. Flexible and highly controllable aspects enable the systematic and thorough investigation of the intriguing interplay between different mechanisms closely related to the spin dynamics of the high-spin systems in optical lattices.

In this work, we theoretically investigate the spin dynamics of fermionic high-spin atoms in the optical superlattice, which involves both spin-changing interactions and tunneling. By tuning the depth of the potential, we simulate the time evolution of the relative populations, starting from the initial band insulator, in several typical parameter regions. By applying perturbation analysis to the interplay between spin-changing interaction and tunneling, we obtain analytical expressions of these population oscillations, which are in excellent agreement with the numerical results. When the spin-changing strength and tunneling strength are comparable, the spin dynamics feature a spin-changing oscillation with the amplitude modulated by the superexchange interaction. In the very deep and very shallow double-well potentials, the spin dynamics feature simple harmonic oscillations with the oscillation frequencies related only to the spin-changing strength. However, their mechanisms are essentially different, with tunneling scarcely contributing in the former and playing a significant role in the spin dynamics of the latter. The latter case can be properly explicated with the perturbation model. These results pave the way for the exploration of more sophisticated spin dynamics with high-spin atoms in optical lattices.

For high-spin particles, spin-changing collisions can change the spin configuration of the atoms. When two atoms with the spin configuration (m_1, m_2) collide and are transferred into a new spin configuration, (m_3, m_4), the process must conserve the total magnetization $(m_1 + m_2 = m_3 + m_4)$ and obey the Pauli exclusion principle ($m_1 \neq m_2$ and $m_3 \neq m_4$). If tunneling couplings simultaneously exist in the system, the resulting spin-changing dynamics will be quite different because of the interplay between the two types of couplings. We consider four fermionic high-spin atoms trapped in the optical superlattice. Suppose that the initial state is appropriately selected such that there is only one spin-changing channel $[(m_1, m_2) \leftrightarrow (m_3, m_4)]$ in the dynamical evolution. The system can be described by the Hamiltonian ($\hbar = 1$):

$$\hat{H} = -\sum_{\langle j,i\rangle m} J(\hat{c}^{\dagger}_{im}\hat{c}_{jm} + \text{h.c.}) + \sum_{jm}\frac{U}{2}\hat{n}_{jm}(\hat{n}_{jm} - 1) + V_c\sum_{j}(\hat{c}^{\dagger}_{jm_3}\hat{c}^{\dagger}_{jm_4}\hat{c}_{jm_2}\hat{c}_{jm_1} + \text{h.c.}), \quad (1)$$

where $j = L, R$ denotes the left and right well, respectively; $\hat{c}^{\dagger}_{jm}$ and $\hat{c}_{jm}$ create and annihilate an atom with spin $m(m = m_1, m_2, m_3, m_4)$ in the corresponding well, respectively; $\hat{n}_{jm}$ is the corresponding particle number operator; J, U, and V_c are the tunneling strength, onsite interaction strength of two atoms, and spin-changing strength, respectively; h.c. represents the Hermitian conjugate. The couplings between the quantum states are shown in Fig. 1. We suppose that the initial state is properly selected and the magnetic field is appropriately set such that the energy differences between states can be omitted in each level manifold depicted in Fig. 1[8]. The states in which four atoms occupy the same sites are omitted by appropriately selecting the lattice parameters to make their energies much higher than that of the others and other energy scales. The states which are only occupied by much higher order processes are not included. The Hamiltonian [Eq. (1)] can be written in the form of a matrix with the basis $\{|1\rangle, |2\rangle, ..., |16\rangle\}$ as follows:

$$\begin{pmatrix} M_{11} & M_{12} \\ M_{21} & M_{22} \end{pmatrix}, \tag{2}$$

$$M_{11} = \begin{pmatrix} 0 & 0 & V_c & 0 & 0 & 0 & 0 & V_c \\ 0 & 0 & V_c & 0 & 0 & 0 & 0 & V_c \\ V_c & V_c & 0 & 0 & 0 & 0 & 0 & 0 \\ 0 & 0 & 0 & 0 & 0 & 0 & 0 & 0 \\ 0 & 0 & 0 & 0 & 0 & 0 & 0 & 0 \\ 0 & 0 & 0 & 0 & 0 & 0 & 0 & 0 \\ 0 & 0 & 0 & 0 & 0 & 0 & 0 & 0 \\ V_c & V_c & 0 & 0 & 0 & 0 & 0 & 0 \end{pmatrix},$$

$$M_{12} = M_{21}^{T} = \begin{pmatrix} 0 & 0 & 0 & 0 & 0 & 0 & 0 & 0 \\ 0 & 0 & 0 & 0 & 0 & 0 & 0 & 0 \\ -J & J & 0 & 0 & -J & J & 0 & 0 \\ J & 0 & J & 0 & J & 0 & J & 0 \\ -J & 0 & 0 & J & 0 & J & -J & 0 \\ 0 & J & -J & 0 & -J & 0 & 0 & J \\ 0 & -J & 0 & -J & 0 & -J & 0 & -J \\ 0 & 0 & -J & J & 0 & 0 & -J & J \end{pmatrix},$$

$$M_{22} = \mathrm{diag}\,(\,U \quad U \quad U \quad U \quad U \quad U \quad U \quad U\,).$$

Here, we have selected the energy level of state $|1\rangle$ as the zero of energy.

We consider the time evolution of the particles in a double-well potential with depths ranging from very deep to very shallow. For the realistic case, V_c is usually 2 orders of magnitude smaller than U[8]. For simplicity, we assume an amplitude of $V_c = 0.01\,U$, which is consistent with Ref. [8]. We assume that the system is initially prepared in the band-insulating state $|1\rangle$. Then, we monitor the relative populations of state $|1\rangle$ and state $|2\rangle$ during the time evolution. For symmetry considerations, we take the difference between the relative populations of these two states [$N(t) = P_1(t) - P_2(t)$, where $P_{1,2}(t)$ is the relative population of the state $|1\rangle, |2\rangle$] to obtain the evolution curves. The results are presented in Fig. 2.

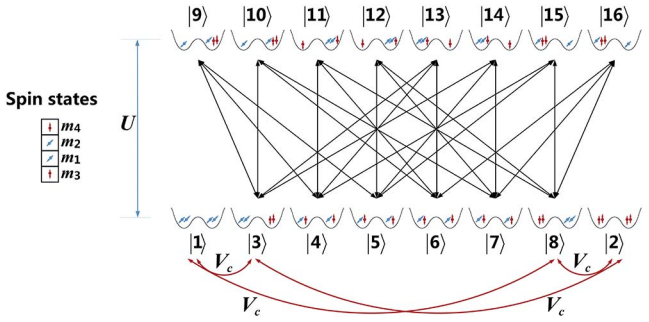

Fig. 1. Schematic of the couplings between the quantum states. The black arrows represent the tunneling couplings, and the red arrows represent the spin-changing couplings. The spin states for the atoms are shown (left). All of the coupling strengths (coupling matrix elements) are provided in Eq. (2).

In the very deep double-well potential, the result [green dashed line in Fig. 2(a)] appears as a simple harmonic oscillation. In this case, we have $|U| \gg |V_c| \gg |J|$. The tunneling couplings are very weak and far-off-resonant, whereas the spin-changing couplings are strong and resonant. Thus, the system is clearly dominated by the spin-changing couplings. For simplicity, we can omit the high-order effect originating from the tunneling

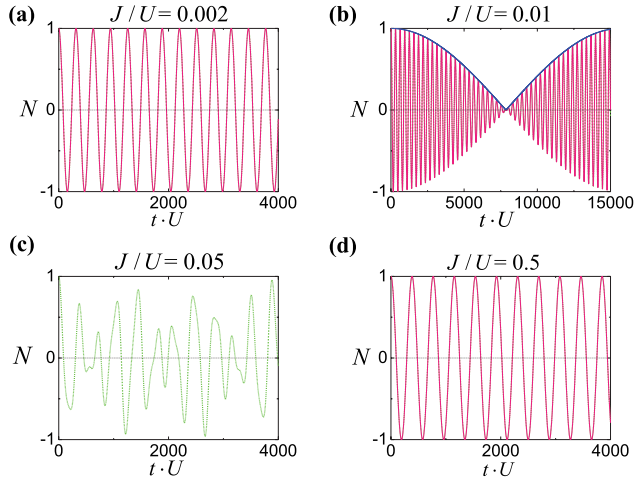

Fig. 2. Time evolution of the difference between the relative populations of states $|1\rangle$ and $|2\rangle$ for amplitudes (a) $J/U = 0.002$, (b) $J/U = 0.01$, (c) $J/U = 0.05$, and (d) $J/U = 0.5$. For all four cases, $V_c/U = 0.01$. The green dashed lines were obtained through numerical simulation with the Hamiltonian. The red solid lines were obtained using analytical methods and correspond to (a) $\cos(2\,V_c t)$, (b) $\cos(J_{\mathrm{ex}} t)\cos(2\,V_c t)$, and (d) $\cos(2\sqrt{2/3}\,V_c t)$. The blue solid line in (b) is the modulation envelope obtained using the analytical method, which corresponds to $\cos(J_{\mathrm{ex}} t)$.

couplings, and hence, the system can be simplified as a four-level system with all four states ($|1\rangle$, $|2\rangle$, $|3\rangle$, and $|8\rangle$) being degenerate. Then, through analytical calculation, we can obtain the following analytical expression:

$$N(t) = \cos(2V_c t). \tag{3}$$

This analytical result is depicted as the red solid line in Fig. 2(a), which is in excellent agreement with the numerical results (green dashed line).

When the double-well potential become shallower, the results become slightly more sophisticated. We concentrate on the situation where J and V_c are comparable. The result is depicted by the green dashed line in Fig. 2(b), which appears as a fast oscillation whose amplitude is modulated by a cosine envelope. To quantitatively understand this phenomenon, we then use the perturbation method to obtain an analytical expression. Under this circumstance, the tunneling couplings are far-off-resonant. Thus, we can adiabatically eliminate the states in which one of the double-well sites contains three atoms and the other site contains one atom ($|9\rangle$–$|16\rangle$ in Fig. 1). The system can thus be simplified in the low-energy-state space [Fig. 3(a)]. In this reduced state space, the original one-order tunneling couplings are transformed into superexchange couplings (green arrows; $J_{\rm ex} = 2J^2/U$ is defined as the superexchenge coupling strength[33–35]). The Hamiltonian matrix in the reduced state space ($\{|1\rangle, |2\rangle, ..., |8\rangle\}$) can be written as follows:

$$\begin{pmatrix}
0 & 0 & V_c & 0 & 0 & 0 & 0 & V_c \\
0 & 0 & V_c & 0 & 0 & 0 & 0 & V_c \\
V_c & V_c & -2J_{\rm ex} & J_{\rm ex} & -J_{\rm ex} & -J_{\rm ex} & J_{\rm ex} & 0 \\
0 & 0 & J_{\rm ex} & -2J_{\rm ex} & J_{\rm ex} & J_{\rm ex} & 0 & J_{\rm ex} \\
0 & 0 & -J_{\rm ex} & J_{\rm ex} & -2J_{\rm ex} & 0 & J_{\rm ex} & -J_{\rm ex} \\
0 & 0 & -J_{\rm ex} & J_{\rm ex} & 0 & -2J_{\rm ex} & J_{\rm ex} & -J_{\rm ex} \\
0 & 0 & J_{\rm ex} & 0 & J_{\rm ex} & J_{\rm ex} & -2J_{\rm ex} & J_{\rm ex} \\
V_c & V_c & 0 & J_{\rm ex} & -J_{\rm ex} & -J_{\rm ex} & J_{\rm ex} & -2J_{\rm ex}
\end{pmatrix}. \tag{4}$$

In this case, we have $|V_c| \gg |J_{\rm ex}|$. Hence, in this reduced space, all the spin-changing couplings are relatively strong and near-resonant, whereas all the superexchange couplings are relatively weak and resonant. Compared with the spin-changing couplings, the superexchange couplings can be viewed as the perturbation. We then diagonalize the reduced Hamiltonian matrix without including the perturbation, and the resulting energy levels of the eigenstates are grouped into several manifolds [Fig. 3(b)]. In the model of Fig. 3(b), the original superexchange couplings [Fig. 3(a)] are transformed into new forms with the order of magnitude still being $|J_{\rm ex}|$. The Hamiltonian matrix in the new basis ($\{|\alpha\rangle, |\beta\rangle, |\xi\rangle, |\eta\rangle, |4\rangle, |5\rangle, |6\rangle, |7\rangle\}$) is

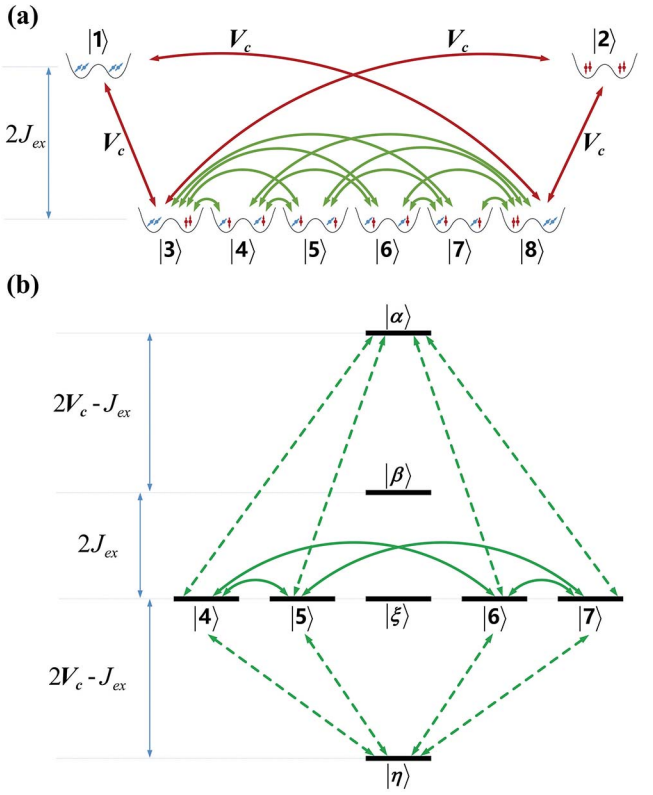

Fig. 3. (a) Schematic of the couplings between the quantum states in the reduced state space. The red solid arrows and green solid arrows represent the spin-changing couplings and superexchange couplings, respectively. (b) Schematic of the couplings between the quantum states in the state space that originates from the perturbation treatment of the reduced states space. The green solid arrows and green dashed arrows represent the resonant couplings and far-off-resonant couplings, respectively, that both originate from the transformation of the superexchange couplings.

$$\begin{pmatrix}
2V_c - J_{\rm ex} & 0 & 0 & 0 & J_{\rm ex} & -J_{\rm ex} & -J_{\rm ex} & J_{\rm ex} \\
0 & 0 & 0 & 0 & 0 & 0 & 0 & 0 \\
0 & 0 & -2J_{\rm ex} & 0 & 0 & 0 & 0 & 0 \\
0 & 0 & 0 & -2V_c - J_{\rm ex} & J_{\rm ex} & -J_{\rm ex} & -J_{\rm ex} & J_{\rm ex} \\
J_{\rm ex} & 0 & 0 & J_{\rm ex} & -2J_{\rm ex} & J_{\rm ex} & J_{\rm ex} & 0 \\
-J_{\rm ex} & 0 & 0 & -J_{\rm ex} & J_{\rm ex} & -2J_{\rm ex} & 0 & J_{\rm ex} \\
-J_{\rm ex} & 0 & 0 & -J_{\rm ex} & J_{\rm ex} & 0 & -2J_{\rm ex} & J_{\rm ex} \\
J_{\rm ex} & 0 & 0 & J_{\rm ex} & 0 & J_{\rm ex} & J_{\rm ex} & -2J_{\rm ex}
\end{pmatrix}. \tag{5}$$

The definitions of the relevant states are

$$|\alpha\rangle = (|1\rangle + |2\rangle + |3\rangle + |8\rangle)/2,$$
$$|\beta\rangle = (-|1\rangle + |2\rangle)/\sqrt{2},$$
$$|\xi\rangle = (-|3\rangle + |8\rangle)/\sqrt{2},$$
$$|\eta\rangle = (-|1\rangle - |2\rangle + |3\rangle + |8\rangle)/2. \quad (6)$$

The couplings between the states in the same manifold are resonant, whereas the other couplings are far-off-resonant. Fortunately, the initial state $[|1\rangle = (-|\alpha\rangle - \sqrt{2}|\beta\rangle + |\eta\rangle)/2]$ has nonzero overlaps with the only three states ($|\alpha\rangle$, $|\beta\rangle$, $|\eta\rangle$) that are not coupled to other states through near-resonant or resonant coupling. Thus, without considering the higher-order effect induced by the far-off-resonant couplings, the system can be simplified as a three-level system. Then, through analytical calculation, we can obtain the following final analytical expression:

$$N(t) = \cos(J_{\rm ex}t)\cos(2V_c t). \quad (7)$$

This analytical result is depicted as the red solid line in Fig. 2(b), which is in excellent agreement with the numerical result (green dashed line). It is now clear that the fast oscillation corresponds to the spin-changing collision, whose amplitude is modulated by an envelope [blue solid line in Fig. 2(b)] that is mainly induced by superexchange. In fact, the result obtained in the very deep double-well potential [Fig. 2(a)] also satisfies the analytical expression presented in Eq. (7). The difference is that in the very deep double-well potential, we have $\cos(J_{\rm ex}t) \sim 1$.

When we continue to decrease the depth of the potential, the resulting oscillation curve behaves in a somewhat complicated manner, as observed in Fig. 2(c). In this situation, the tunneling couplings and spin-changing couplings together contribute to the complicated oscillation. As observed in Fig. 2(c), the phase of the resulting oscillation is not uniform; thus, there is no simple analytical expression for this situation.

Next, we focus on the spin dynamics in the very shallow double-well potential. The result is presented as the green dashed line in Fig. 2(d), which involves a very simple oscillation. To quantitatively understand this oscillation, we use the perturbation method to obtain an analytical expression. In this case, we have $|V_c| \ll |J|, |U|$. The tunneling couplings are near-resonant, and the spin-changing couplings are resonant. Compared with the strong tunneling couplings, the weak spin-changing couplings can be viewed as the perturbation. At first, we diagonalize the Hamiltonian without including the perturbation, and the resulting energy levels of the eigenstates are grouped into six manifolds that are well separated from each other (Fig. 4). In the manifold that includes the initial state ($|1\rangle$), the states are degenerate; thus, there are free parameters when we construct the orthogonal states. For simplicity, we construct the orthogonal states to ensure that one of the superposition states ($|\alpha 1\rangle$) is coupled to the two bare states ($|1\rangle$ and $|2\rangle$) and the other ($|\alpha 2\rangle$) is

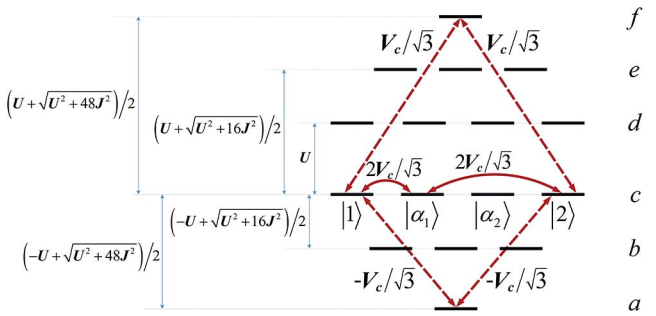

Fig. 4. Schematic of the couplings between the quantum states in the state space that originates from the perturbation treatment of the original state space. The red solid arrows and red dashed arrows represent the resonant couplings and far-off-resonant couplings, respectively, that both originate from the transformation of the spin-changing couplings.

not, i.e., $|\alpha 1\rangle = (2|3\rangle + |4\rangle - |5\rangle - |6\rangle + |7\rangle + 2|8\rangle)/(2\sqrt{3})$ and $|\alpha 2\rangle = (|4\rangle + |5\rangle + |6\rangle + |7\rangle)/2$. These four states are not coupled to the other states through near-resonant or resonant coupling. Thus, starting from state $|1\rangle$, without considering the higher-order effect induced by the far-off-resonant couplings, the spin dynamics occur only in a few states ($|1\rangle$, $|2\rangle$, $|\alpha 1\rangle$). (State $|\alpha 2\rangle$ does not need to be considered because it is not coupled to any state.) The following final analytical expression is obtained:

$$N(t) = \cos\left(2\sqrt{\frac{2}{3}}V_c t\right). \quad (8)$$

This analytical result is depicted as the red solid line in Fig. 2(d), which is consistent with the numerical result (green dashed line). According to the analytical expression, the oscillation parameter is only related to the spin-changing strength. This result is not intuitive in the original coupling model (Fig. 1); however, it is apparent in the perturbation model (Fig. 4), in which all the relevant states ($|1\rangle$, $|2\rangle$, $|\alpha 1\rangle$) are degenerate and connected only by the spin-changing couplings. Although the oscillation parameter is unrelated to the tunneling strength, the spin dynamics comprise both spin-changing and tunneling, which can be observed more clearly by examining the noticeable populations of the states that are only connected by the tunneling couplings [see Fig. 5(a)]. This situation is essentially different from the case of a very deep double-well potential [Fig. 5(b)], in which the tunneling scarcely contributes.

From the experimental viewpoint, we can prepare ^{40}K in the $f = 9/2$ manifold[8] to achieve the spin dynamics proposed in this Letter. For the initial state, we suggest a mixture of $|m_1, m_2\rangle = |1/2, 9/2\rangle$, which is coupled only to $|3/2, 7/2\rangle$. The state $|5/2, 5/2\rangle$ is forbidden because of Pauli blocking. The magnetic field for realizing resonant spin-changing oscillation is on the order of magnitude of 100 mG[8]. Techniques for obtaining an optical double-well potential[29,31], as well as preparing an initial band

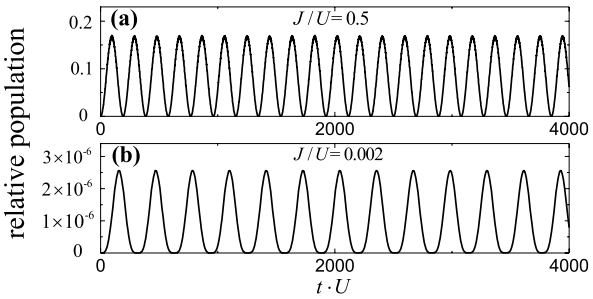

Fig. 5. Time evolution of the summary of the relative populations of several states ($|4\rangle$, $|5\rangle$, $|6\rangle$, and $|7\rangle$) that are only connected by the tunneling couplings for the (a) very shallow and (b) very deep double-well potential cases. For both cases, $V_c/U = 0.01$. The results were obtained through numerical simulation with the Hamiltonian. The other states ($|9\rangle$–$|16\rangle$) are scarcely populated during the evolution for both cases and are not depicted in the figures. For the very shallow double-well potential, the relevant populations are noticeable, which indicates that tunneling plays an important role in the spin dynamics. In contrast, for the very deep double-well potential, the relevant populations are inconspicuous, which indicates that tunneling scarcely contributes.

insulator and detecting relative populations of different states[8], have been successfully developed.

In conclusion, we systematically investigate the spin dynamics of fermionic high-spin atoms in optical superlattices. Through numerical simulations using the Hamiltonian and analytical calculations involving the interplay between the spin-changing interactions and tunneling, we determine the time evolution behavior of an initially band-insulating state in a potential with very deep to very shallow depths. The numerical results and analytical results show excellent agreement. When the spin-changing strength and tunneling strength are comparable, the spin dynamics are characterized by modulated oscillation, with the fast oscillation frequency corresponding to the spin-changing strength and the modulation envelope corresponding to the superexchange strength. When the potential depth is very deep or very shallow, the spin dynamics feature simple harmonic oscillation with the oscillation frequency relates only to the spin-changing strength. Tunneling scarcely contributes for the very deep potential depth but is indispensable for the very shallow case. We expect similar results for fermionic high-spin atoms in certain other systems, where more sophisticated and intriguing phenomena are desired.

This work was supported by the National Key Research and Development Program of China under Grant No. 2016YFA0301504.

References

1. I. Bloch, J. Dalibard, and W. Zwerger, Rev. Mod. Phys. **80**, 885 (2008).
2. M. Lewenstein, A. Sanpera, and V. Ahufinger, *Ultracold Atoms in Optical Lattices: Simulating Quantum Many-Body Systems* (Oxford University, 2012).
3. S. Deachapunya and S. Srisuphaphon, Chin. Opt. Lett. **12**, 031101 (2014).
4. Q. Xu, H. Liu, B. Lu, Y. Wang, M. Yin, D. Kong, J. Ren, X. Tian, and H. Chang, Chin. Opt. Lett. **13**, 100201 (2015).
5. T. Lompe, T. B. Ottenstein, F. Serwane, A. N. Wenz, G. Zurn, and S. Jochim, Science **330**, 940 (2010).
6. S. Taie, Y. Takasu, S. Sugawa, R. Yamazaki, T. Tsujimoto, R. Murakami, and Y. Takahashi, Phys. Rev. Lett. **105**, 190401 (2010).
7. S. Stellmer, R. Grimm, and F. Schreck, Phys. Rev. A **84**, 043611 (2011).
8. J. S. Krauser, J. Heinze, N. Flaschner, S. Gotze, O. Jurgensen, D. S. Luhmann, C. Becker, and K. Sengstock, Nat. Phys. **8**, 813 (2012).
9. O. Jurgensen, J. Heinze, and D. S. Luhmann, New J. Phys. **15**, 113017 (2013).
10. T. L. Ho, Phys. Rev. Lett. **81**, 742 (1998).
11. C. K. Law, H. Pu, and N. P. Bigelow, Phys. Rev. Lett. **81**, 5257 (1998).
12. T. Ohmi and K. Machida, J. Phys. Soc. Jpn. **67**, 1822 (1998).
13. N. Bornemann, P. Hyllus, and L. Santos, Phys. Rev. Lett. **100**, 205302 (2008).
14. J. S. Krauser, U. Ebling, N. Flaschner, J. Heinze, K. Sengstock, M. Lewenstein, A. Eckardt, and C. Becker, Science **343**, 157 (2014).
15. T. L. Ho and S. Yip, Phys. Rev. Lett. **82**, 247 (1999).
16. C. J. Wu, J. P. Hu, and S. C. Zhang, Phys. Rev. Lett. **91**, 186402 (2003).
17. C. J. Wu, Phys. Rev. Lett. **95**, 266404 (2005).
18. P. Lecheminant, E. Boulat, and P. Azaria, Phys. Rev. Lett. **95**, 240402 (2005).
19. H. H. Tu, G. M. Zhang, and L. Yu, Phys. Rev. B **74**, 174404 (2006).
20. A. Rapp, G. Zarand, C. Honerkamp, and W. Hofstetter, Phys. Rev. Lett. **98**, 160405 (2007).
21. K. Rodriguez, A. Arguelles, M. Colome-Tatche, T. Vekua, and L. Santos, Phys. Rev. Lett. **105**, 050402 (2010).
22. C. Honerkamp and W. Hofstetter, Phys. Rev. Lett. **92**, 170403 (2004).
23. A. V. Gorshkov, M. Hermele, V. Gurarie, C. Xu, P. S. Julienne, J. Ye, P. Zoller, E. Demler, M. D. Lukin, and A. M. Rey, Nat. Phys. **6**, 289 (2010).
24. X. Zhang, M. Bishof, S. L. Bromley, C. V. Kraus, M. S. Safronova, P. Zoller, A. M. Rey, and J. Ye, Science **345**, 1467 (2014).
25. F. Scazza, C. Hofrichter, M. Höfer, P. C. De Groot, I. Bloch, and S. Folling, Nat. Phys. **10**, 779 (2014).
26. G. Cappellini, M. Mancini, G. Pagano, P. Lombardi, L. Livi, M. Siciliani de Cumis, P. Cancio, M. Pizzocaro, D. Calonico, F. Levi, C. Sias, J. Catani, M. Inguscio, and L. Fallani, Phys. Rev. Lett. **113**, 120402 (2014).
27. M. A. Cazalilla and A. M. Rey, Rep. Prog. Phys. **77**, 124401 (2014).
28. M. Greiner, O. Mandel, T. Esslinger, T. W. Hänsch, and I. Bloch, Nature **415**, 39 (2002).
29. S. Fölling, S. Trotzky, P. Cheinet, M. Feld, R. Saers, A. Widera, T. Muller, and I. Bloch, Nature **448**, 1029 (2007).
30. A. M. Rey, V. Gritsev, I. Bloch, E. Demler, and M. D. Lukin, Phys. Rev. Lett. **99**, 140601 (2007).
31. S. Trotzky, P. Cheinet, S. Fölling, M. Feld, U. Schnorrberger, A. M. Rey, A. Polkovnikov, E. A. Demler, M. D. Lukin, and I. Bloch, Science **319**, 295 (2008).
32. R. C. Brown, R. Wyllie, S. B. Koller, E. A. Goldschmidt, M. Foss-Feig, and J. V. Porto, Science **348**, 540 (2015).
33. L. M. Duan, E. Demler, and M. D. Lukin, Phys. Rev. Lett. **91**, 090402 (2003).
34. E. Altman, W. Hofstetter, E. Demler, and M. D. Lukin, New J. Phys. **5**, 113 (2003).
35. A. B. Kuklov and B. V. Svistunov, Phys. Rev. Lett. **90**, 100401 (2003).